AD-A087 948 RICE UNIV HOUSTON TX F/G 4/1
QUANTITATIVE SIMULATION OF A MAGNETOSPHERIC SUBSTORM. 3. PLASMA--ETC(U)
JAN 80 R W SPIRO, M HAREL, R A WOLF F19628-77-C-0005
UNCLASSIFIED SCIENTIFIC-4 AFGL-TR-80-0130 NL

1 OF 1
AD A087948

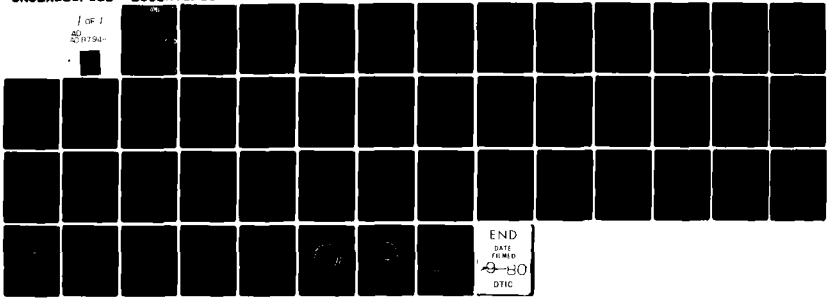

END
DATE FILMED
9-80
DTIC

AFGL-TR-80-0130

LEVEL II

AD A087948

QUANTITATIVE SIMULATION OF A MAGNETOSPHERIC SUBSTORM
3. Plasmaspheric Electric Fields and Evolution of the Plasmapause

R. W. Spiro
M. Harel
R. A. Wolf
P. H. Reiff

William Marsh Rice University
6100 South Main Street
Houston, Texas 77005

Scientific Report , No. 4

25 January 1980

Approved for public release; distribution unlimited

AIR FORCE GEOPHYSICS LABORATORY
AIR FORCE SYSTEMS COMMAND
UNITED STATES AIR FORCE
HANSCOM AFB, MASSACHUSETTS 01731

Unclassified
SECURITY CLASSIFICATION OF THIS PAGE (When Data Entered)

SCIENTIFIC-4

REPORT DOCUMENTATION PAGE	READ INSTRUCTIONS BEFORE COMPLETING FORM
1. REPORT NUMBER: AFGL-TR-80-0130	2. GOVT ACCESSION NO.: AD-A087948
3. RECIPIENT'S CATALOG NUMBER	
4. TITLE (and Subtitle): Quantitative Simulation of a Magnetospheric Substorm, 3. Plasmaspheric Electric Fields and Evolution of the Plasmapause.	5. TYPE OF REPORT & PERIOD COVERED: Scientific Report No. 4
	6. PERFORMING ORG. REPORT NUMBER
7. AUTHOR(s): R. W. Spiro, M. Harel, R. A. Wolf and P. H. Reiff	8. CONTRACT OR GRANT NUMBER(s): F19628-77-C-0005
9. PERFORMING ORGANIZATION NAME AND ADDRESS: William Marsh Rice University, 6100 South Main St., Houston, TX 77005	10. PROGRAM ELEMENT, PROJECT, TASK AREA & WORK UNIT NUMBERS: 61102F 2311
11. CONTROLLING OFFICE NAME AND ADDRESS: U.S. Air Force Geophysics Laboratory, Hanscom AFB, Massachusetts 01731, Contract Monitor: Capt. David Hardy (PHG)	12. REPORT DATE: 25 January 1980
	13. NUMBER OF PAGES: 46
14. MONITORING AGENCY NAME & ADDRESS (if different from Controlling Office)	15. SECURITY CLASS. (of this report): Unclassified
	15a. DECLASSIFICATION DOWNGRADING SCHEDULE

16. DISTRIBUTION STATEMENT (of this Report)

Approved for public release; distribution unlimited

17. DISTRIBUTION STATEMENT (of the abstract entered in Block 20, if different from Report)

18. SUPPLEMENTARY NOTES

19. KEY WORDS (Continue on reverse side if necessary and identify by block number)

Magnetosphere
Ionosphere
Plasmasphere
Electric Fields

20. ABSTRACT (Continue on reverse side if necessary and identify by block number)

Results of the Rice University substorm simulation have been used to investigate the penetration of substorm-associated electric fields into the plasmasphere. Near 4 R_E in the equatorial plane, our time-dependent electric field model is characterized by eastward components in the dusk-midnight local time sector and westward components after midnight. Except for a small region just before dusk the model predicts eastward electric field components throughout the daytime sector. The characteristic radial component is directed

DD FORM 1 JAN 73 1473 EDITION OF 1 NOV 65 IS OBSOLETE

Unclassified
SECURITY CLASSIFICATION OF THIS PAGE (When Data Entered)

inward at all local times except for a small region just after dawn. These results compare favorably with available whistler and incoherent scatter measurements obtained during magnetically disturbed periods.

By assuming an initial plasmapause shape and by following the computed $\underline{E} \times \underline{B}$ drift trajectories of plasma flux tubes from that initial boundary we have examined the short-term evolution of the plasmapause during the substorm-like event of 19 September 1976. We find that narrow filamentary tails can be drawn out from the plasmasphere near dusk within hours of substorm onset. These tail-like appendages to the plasmasphere subsequently drift rapidly from the dusk sector toward the daytime magnetopause.

Investigation of the large-scale time-dependent flow of plasma in the evening sector indicates that some mid-latitude plasma flux tubes that drift eastward past the dusk terminator reverse their motion between dusk and midnight and begin to drift westward toward dusk. Such time-dependent changes in flow trajectories may be related to the formation of F-region ionization troughs.

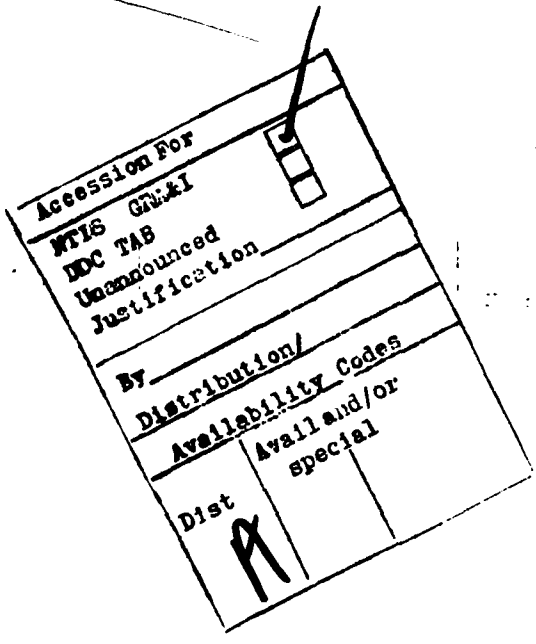

I. INTRODUCTION

Quantitative models of plasma flow in the magnetosphere-ionosphere system have shown that plasma-sheet particles can shield the inner magnetosphere from most of the effects of the magnetospheric convection electric field [Karlson, 1963, 1971; Block, 1966; Vasyliunas, 1970, 1972; Swift, 1971; Jaggi and Wolf, 1973; Harel and Wolf, 1976; Harel et al. 1980a, b]. As a result, corotation with the earth dominates thermal plasma flow in the middle and low latitude regions of the ionosphere, while the magnetospheric convection electric field dominates the higher latitude polar cap and auroral regions [Mozer, 1973]. The characteristic time scale for shielding to occur depends on both ionospheric and plasma-sheet properties with estimates ranging from a few minutes to several hours [Jaggi and Wolf, 1973].

During times of rapid change in the magnetosphere-ionosphere system (such as during substorms), the shielding mechanisms are ineffective and magnetospheric electric fields penetrate into the plasmasphere. Experimental results indicate that mid-latitude electric fields measured during magnetically disturbed periods differ sustantially from measurements made during quiet periods [Blanc, 1978; Park, 1978; Carpenter and Seely, 1976; Carpenter et al., 1979].

In this paper we use the results of the quantitative substorm simulation described by Harel et al., [1980a, b] (hereafter referred to as Paper 1 and Paper 2, respectively) to investigate the penetration of substorm-associated electric fields into the plasmasphere and mid-latitude ionosphere. We first examine the computed spatial and

temporal variations of the plasmaspheric electric field through the course of the modeled event. These results, calculated for a specific event, are then compared with available whistler and incoherent scatter radar results obtained during magnetically disturbed periods. Finally, we use the time-dependent substorm electric field model to examine two geophysical phenomena that depend critically on global electric field configuration: the temporal evolution of the plasmapause and the formation of F-region ionization troughs.

II. SUBSTORM-ASSOCIATED ELECTRIC FIELDS IN THE PLASMASPHERE

The inner magnetosphere modeling program described in Paper 1 uses certain initial and boundary conditions to compute self-consistent electric fields, electric currents, and plasma motions in the ionosphere and in the magnetospheric equatorial plane. Unless otherwise noted, the electric field results used in this paper are described in Table 2 of Paper 1 as "Run 1".

Calculated electric field ($\underline{E}$) patterns at six different times during the simulated event are shown in Figures 1 and 2. Figure 1 shows the east-west component of electric field at 4 R_E in the equatorial plane of the magnetosphere, while Figure 2 shows the radial component of $\underline{E}$. Computed electric field patterns are shown as a function of magnetic local time for the following times: (1) the end of the quiet period before the substorm growth phase (0900 UT), (2) just before substorm onset (1000-εUT), (3) just after substorm onset (1000+εUT), (4) the time of substorm maximum (1050 UT), (5) the time of maximum measured cross-polar-cap potential drop

(1150 UT), and (6) a time well into the recovery phase of the substorm (1300 UT). (See Figure 3 of Paper 1). The electric field components in Figures 1 and 2 are shown in a reference frame that corotates with the earth. The plotted components do, however, include the effects of induction fields that result from temporal changes in the magnetic field model.

The 0900 UT results were obtained by allowing the inner magnetosphere modeling program to relax for two hours magnetospheric time using time-independent input parameters. During this period the system did not completely relax to a "steady state." Although Figures 1 and 2 show that shielding of the inner magnetosphere at 4 R_E is almost complete at 0900 UT on the night side of the earth, electric field components of more than .1 mV/m are still evident on the dayside.

Turning our attention first to the east-west electric field components shown in Figure 1, we note that there is a repeatable pattern of electric field reversals throughout the simulated event. In general, the midnight-dawn local time sector is a region of westward electric field (inward $\underline{E} \times \underline{B}$ plasma drift), while the daytime sector is a region of eastward electric field. The post-dusk sector is a region of eastward field that is separated from the daytime eastward field pattern by a narrow sector of small or westward field located just before dusk.

The magnitudes of the field components shown in Figures 1 and 2 depend in a complicated way on the degree of shielding and on the instantaneous value of the cross-polar-cap potential drop. The maximum nighttime electric fields occur immediately following the sudden

enhancement in auroral zone conductivity that marks the substorm onset at 1000+ε UT. The daytime field components on the other hand do not show as much variation.

The radial E field components shown in Figure 2 reveal that the entire dusk sector from noon to midnight is characterized by outward-directed electric field (westward plasma drift) except during the period of substorm recovery (1300 UT). Immediately after substorm onset (1000+ε UT) the dawn sector (midnight to noon) is a region of inward-directed electric field (eastward $\underline{E} \times \underline{B}$ drift). Later in the event, however, the inward-directed field region is confined to a narrow 4 hour sector centered near 0900 MLT. The midnight-dawn radial electric field after the initial onset is generally less than .1 mV/m and directed outward as in the pre-midnight sector.

Substorm-associated electric fields mapped into the middle and low latitude ionosphere are shown in Figures 3 and 4. Figure 3 shows the east-west component of ionospheric $\underline{E}$ at 1050 UT at latitudes 60°, 50°, 40°, and 30°. Figure 4 shows the north-south component of $\underline{E}$ at the same latitudes. Eastward fields in the equatorial plane map into eastward fields in the ionosphere and radially outward equatorial fields become poleward-directed ionospheric fields. Figures 3 and 4 illustrate the decreasing influence of magnetospheric electric fields at successively lower latitudes.

The electric field configurations shown in Figures 1-4 are considerably different from the predictions of models characterized by uniform dawn-dusk convection electric fields (see review by Kivelson, 1976). A uniform (unshileded) dawn-dusk field would have westward E field components at

night and eastward daytime components. Similarly, such a model would predict inward electric field components on the dawn side of the earth and outward components on the dusk side. The characteristic electric field reversals illustrated in Figures 1-4 result from abrupt changes in height-integrated electrical conductivity at the dawn and dusk terminators. Although he specifically neglected field-aligned currents between the plasma sheet and the ionosphere, Wolf [1970] has shown that ionospheric current continuity at dawn and dusk requires electric equipotentials to be compressed near the dusk polar cap and to be spread apart near the dawn polar cap. The more sophisticated calculations presented here bear out this conclusion as illustrated in Figure 5 which shows the electric equipotential pattern in the equatorial plane at 1050 UT (cf. Figure 2c of [Wolf, 1970]).

III. COMPARISON WITH OBSERVATIONS

Electric fields in the middle and low latitude ionosphere have been measured by a variety of experimental techniques (see review by Evans [1975]). The most extensive investigations of plasmaspheric electric fields during magnetically disturbed periods are based on incoherent scatter radar results fromn St. Santin [Testud et al., 1975; Blanc et al., 1977; Blanc, 1978] and on the cross-L motions of whistler ducts [Park, 1978; Carpenter et al., 1972, 1979]. Evans [1972] has presented Millstone Hill radar results showing westward F-region ion drifts of almost 200 m/sec in the afternoon sector on 14 May, 1969. Testud et al. [1975] have pointed out that the abrupt increase in ion velocity observed

by Evans [1972] occurred at the same time as an abrupt increase in the auroral electrojet (AE) index. Testud et al. [1975] and Blanc et al. [1977] have both presented St. Santin backscatter measurements that show westward and northward drift components near 2100 LT on the night of 30 October 1973. Near midnight on the same night the meridional ion drift component changed from northward to southward, while westward drift (northward $\underline{E}$ field) prevailed throughout the night. These results are in general agreement with the outcome of our event simulation -- poleward and eastward $\underline{E}$ field components before midnight, poleward and westward components after midnight (see Figures 3 and 4).

Park [1978] has used cross-L motions of individual whistler ducts to infer the east-west component of electric field in the nighttime plasmasphere during moderate substorms. He found eastward fields of $\sim$.2 mV/m in the equatorial plane in the pre-midnight sector and westward fields after midnight. His analysis was based on the study of individual cases. Carpenter et al. [1979] have used whistler data acquired on 34 observing days to define an average model of substorm electric field in the plasmasphere near L = 4. Substorm intervals were defined as those in which the AE index exceeded 200γ. Figure 6 shows a harmonic series expansion of the Carpenter et al. [1979] substorm electric field results in the equatorial plane of the magnetosphere. The whistler results shown here were averaged over all substorm phases while our model results presented in Figures 1 and 2 were obtained at specific times during a substorm-like event. In order to compare more directly with the average whistler-inferred electric field data shown in Figure 6, we have averaged our calculated equatorial east-west components at 4 R_E for the

post-growth phase results shown in Figure 1. Both the theoretical and whistler-inferred results show westward electric fields of a few mV/m in the post-midnight local time sector, corresponding to inward $\underline{E} \times \underline{B}$ drift of plasmaspheric flux tubes in the early morning sector. Similarly, both the whistler and theoretical results predict eastward electric fields (outward plasma drifts) in the dusk-midnight sector. The largest disagreement between data and theory occurs near noon where the simulation results are known to be inaccurate as a result of numerical method limitations discussed in Paper 1. It is interesting to note that the region of westward $\underline{E}$ field located just before dusk in the individual plots shown in Figure 1 survives in the time-averaged results of Figure 6.

Nighttime ionosonde data have offered indirect evidence for the electric field pattern shown in Figure 6. Park [1971] and Park and Meng [1971, 1973] have shown that the mid-latitude F-region responds to substorm activity by being pushed upward in the pre-midnight sector and pushed downward after midnight. These authors have interpreted these characteristic shifts as being due to an eastward-directed electric field in the evening and westward-directed field in the early morning.

Blanc [1978] has presented incoherent backscatter measurements of F-region ion drifts during magnetically disturbed periods from the multistatic radar facility at St. Santin. After subtracting quiet-day diurnal variations to remove the effects of atmospheric dynamo electric fields, Blanc [1978] presents two examples of magnetic "perturbation $\underline{E} \times \underline{B}$ drift velocity". These examples show westward $\underline{E} \times \underline{B}$ drift (northward $\underline{E}$ field) in the afternoon and evening local time sectors. In addition to these individual case studies, average $\underline{E} \times \underline{B}$ perturbation drift results

are shown for periods when Kp > 2. Values of northward E scaled from the average drift velocity plot shown in Figure 3 of Blanc [1978] are given in Figure 7 along with the northward E component that results from averaging the post-growth phase electric fields shown in Figure 2. While the radar results show poleward-directed E throughout the day, our results suggest that there is a narrow region of equatorward-directed E (eastward plasma drift) just after dawn. Otherwise, the observations and the theoretical results are very similar. The average north-south plasma drift components measured at St. Santin for Kp > 2 are quite different from the characteristic drift pattern we have calculated however. The St. Santin data suggest that small equatorward drifts (westward E components) are found throughout the pre-midnight sector while our results and the whistler measurements of Carpenter et al. [1979] suggest that this is a region of poleward drift (eastward E field).

Simultaneous electric field measurements made in the equatorial ionosphere and at auroral zone stations have recently been used to examine the complex coupling of the magnetosphere and the low-latitude ionosphere during magnetically disturbed periods [Fejer et al., 1979; Gonzales et al., 1979; Kelley et al., 1979]. On the basis of Jicamarca radar measurements these studies have shown that the low-latitude electric field is affected by substorm activity and by abrupt changes in the north-south component of the interplanetary magnetic field. Specifically, Kelley et al. [1979] have shown that the characteristic equatorial electric field pattern frequently reverses when the IMF turns northward from a steady southerly direction. Presumably during such a circumstance strong convection ceases, and the electric field due to Alfvén

layer shielding dominates in the inner magnetosphere. In addition, Gonzales et al. [1979] have suggested that an increase in the convection electric field can penetrate directly to the low-latitude ionosphere during the early stages of a substorm before Alfvén layer shielding charges build up.

IV. EVOLUTION OF THE PLASMAPAUSE

Whistler results and in situ observations from satellites have shown the existence of an abrupt drop in thermal plasma concentration at a geocentric distance of a few earth radii in the equatorial plane [Carpenter, 1963; Gringauz, 1963; Taylor et al., 1965; Chappell et al., 1970]. This feature, termed the plasmapause, has been identified under steady state conditions with the boundary between plasma flux tubes that drift on closed drift paths around the earth and flux tubes that are periodically emptied as they drift to the magnetopause during the course of magnetospheric convection [Nishida, 1966]. Another view of the plasmapause based on flux tube interchange motions has been presented by Lemaire [1975].

The characteristic time scale for refilling of plasmaspheric flux tubes after they have been emptied is many (6-10) days [Park, 1970]. Changes in the global magnetospheric convection electric field, on the other hand, are characterized by substorm time scales of a few minutes to a few hours. As a result, the outer plasmasphere is usually in a dynamic state of recovery [Carpenter and Park, 1973], and the plasmapause is not necessarily coincident with the last closed flux tube drift path.

Investigations of the temporal evolution of the plasmapause have shown that "plasma tails" or "regions of detached plasma" [Chappell, 1972, 1974] can be pulled out from the dusk bulge region of the plasmasphere during periods of changing electric field [Grebowsky, 1970, 1971; Grebowsky et al., 1974; Chen and Wolf, 1972; Chen and Grebowsky, 1974; Chen et al., 1975]. These investigations have followed the $\underline{E} \times \underline{B}/B^2$ drift motion of the plasmapause by assuming spatially-invariant, time-dependent models of the dawn-dusk convection electric field. Other studies have shown that the average size of the plasmasphere decreases when magnetic activity increases [Binsack, 1967; Carpenter, 1966, 1967; Chappell et al., 1970], although the tendency for plasmapause radius to decrease with increasing Kp is most evident in the midnight-dawn local time sector [Chappell, 1972; Carpenter and Park, 1973].

We have modeled the short-term temporal development of the plasmapause by following the $\underline{E} \times \underline{B}/B^2$ drift trajectories of plasma flux tubes that initially make up the plasmapause boundary. Our approach differs from previous investigations in the electric field model used and in the characteristic time for electric field changes to occur. Our field model allows for changes in $\underline{E}$ to occur on the time scale of minutes, while previous investigations have been limited to the three hour resolution of the Kp index. As pointed out earlier, our more complicated model agrees better with available data, although presently we are limited to modeling the evolution of the plasmapause only during the four hour period of our substorm simulation.

Since we are only able to follow the evolution of the plasmapause for four hours, we have not been able to follow the motion of individual

flux tubes backward in time to determine if they have been drifting on closed drift trajectories for 6-10 days required for a flux tube to be refilled (see for example Grebowsky et al. [1974]). Instead, we assume an initial plasmapause configuration and follow the trajectories of plasma flux tubes from that initial boundary forward in time. Thus, our ability to model the actual evolution of the plasmapause during the event is limited by our knowledge (or lack of knowledge) of the initial configuration of the plasmapause. We return to this point later.

For the present discussion, we take the view that as long as our electric field model is typical of substorm-associated plasmaspheric electric fields (see Figures 6 and 7), we can accurately follow the $\underline{E} \times \underline{B}/B^2$ trajectories of plasma flux tubes. We can then investigate how the plasmapause evolves for several different assumptions about the initial configuration of the plasmapause boundary. Finally, we examine low altitude ion composition data obtained from S3-2 to determine which of our cases most nearly represents the situation of 19 September 1976.

Figure 8 illustrates the time-dependent development of the plasmapause at 1/2 hour intervals from an initial configuration characterized by a mid-afternoon plasmaspheric bulge. The plasmapause shape at 0900 UT was taken to be coincident with the last closed electric equipotential computed at the end of the initial two hour time-independent quiet-time portion of our simulation. This boundary would correspond to the actual plasmapause boundary at 0900 UT if the global electric field pattern had remained steady for many days before the modeled event. During the substorm growth phase (0900 to 1000 UT) the configuration of the plasmapause changes only slightly. However,

following substorm onset at 1000 UT the plasmasphere responds dynamically. By 1030 UT the plasmasphere boundary has begun to contract inward in the midnight-dawn local time sector and the bulge region has begun to drift outward and westward toward the daytime magnetopause. In addition, a second bulge has begun to form near dusk. The early morning compression of the plasmasphere occurs as a result of the westward electric field that characterizes this local time sector (see Figure 1). Similarly, the daytime outward drift results from the large eastward $\underline{E}$ that penetrates to low latitudes near noon. The dusk bulge becomes apparent as a result of the pre-dusk region of westward $\underline{E}$ and the evening sector region of eastward $\underline{E}$ (Figure 1).

By 1100 UT the initial daytime bulge has almost drifted to the magnetopause (assumed to be at ~10 R_E on the dayside), while flow shears have begun to distort the dusk bulge into a tail-like appendage to the plasmasphere that extends from dusk toward noon. In the early morning local time sector the plasmapause continues to be pushed inward.

As time advances the dusk plasma tail extends further and further into the daytime sector. By 1130 UT local field irregularities in the model result in the formation of an additional small-scale plasma tail in the post dusk sector. In general, the effect of substorm-associated electric fields on the nightside is to force the plasmapause in closer to the earth in the post-midnight sector and to move the plasmapause out away from the earth in the pre-midnight sector. These results are different from the predictions of previous investigations that assumed a spatially invariant dawn-dusk electric field. If $\underline{E}$ were uniformly directed from dawn to dusk one would expect the entire nighttime

plasmasphere to be pushed in closer to the earth.

The initial plasmapause configuration illustrated in Figure 8 is associated with the last closed electric equipotential encircling the earth and is indicative of what would be expected after many days of very low geomagnetic activity. However, the substorm-like event discussed here followed a large magnetic storm (Dst ~ -70γ) on the previous day (18 September 1976) suggesting that the temporal development of the plasmapause shown in Figure 8 may not accurately reflect conditions of 19 September 1976. This figure may, however, more accurately represent a "typical" (i.e., isolated) substorm.

The equatorial plasmapause has frequently been associated with the latitudinal location of a sudden decrease in H^+ ion concentration in the topside ionosphere [Taylor et al., 1969; Taylor, 1972; Titheridge, 1976], although this interpretation has recently been questioned [Grebowsky et al., 1978]. S3-2 ion trap data obtained near dusk just after substorm onset at 1010 UT indicate that the transition from H^+ to O^+ dominance in the topside ionosphere at ~1400 km altitude occurs at approximately 55° invariant latitude (F. J. Rich, personal communication). The S3-2 data thus suggest that, as a result of previous magnetic activity, the plasmapause is compressed to near 3 R_E in the equatorial plane at dusk.

Figure 9 illustrates the evolution of the plasmapause for an initial plasmapause boundary located much closer to the earth than shown in Figure 8. The boundary shown in Figure 9 corresponds to the mapping into the equatorial plane of an initial ionospheric boundary located at 55° latitude. A slight post-dusk bulge is apparent by 1100 UT for this case but a tail-like appendage does not form.

Figures 8 and 9 indicate that the evolution of the plasmapause in response to substorm-associated changes in $\underline{E}$ depends on the initial configuration of the boundary. If the initial plasmasphere extends to near the instantaneous last closed equipotential then plasma tails can form near dusk. If the plasmapause is contracted, however, in response to earlier magnetic activity then the shape of the plasmapause becomes distorted but tails may not form.

V. FORMATION OF THE F-REGION IONIZATION TROUGH

The mid-latitude (or main) ionization trough is a latitudinally narrow region of reduced ionospheric plasma concentration located just equatorward of the nighttime auroral zone [Muldrew, 1965; Sharp, 1966]. Recent theoretical studies of the high latitude ionosphere have suggested that the trough may form within a narrow region of enhanced plasma recombination associated with rapid plasma flow [Banks et al., 1974; Schunk et al., 1975, 1976]. In addition to this view, it has also been suggested that the trough forms not as the result of enhanced plasma recombination in a region of rapid plasma drift, but as the result of the longer time available for plasma recombination to occur in a region of very slow plasma drift [Knudsen, 1974; Watkins, 1978; Spiro et al., 1978].

In particular, Spiro et al. [1978] have used simultaneous measurements of bulk ion flow and total ion concentration to show that the poleward portion of the trough is frequently located in a region of westward plasma drift while the equatorward portion of the trough is located in a region of eastward drift. These observations were interpreted as suggesting that

the F-region trough is formed on mid-latitude plasma flux tubes that have corotated eastward past the dusk terminator before stagnating and reversing their flow to westward in the post-dusk sector.

In order to illustrate that such a nighttime plasma flow geometry would lead naturally to the formation of ionization troughs, Spiro et al. [1978] adopted an ad hoc time-independent model of the total convection electric field including the effects of corotation. The essential feature of the resulting $\underline{E} \times \underline{B}/B^2$ velocity flow field was the location of a flow stagnation point in the post-dusk sector. Whistler results of Carpenter [1970] indicate that the plasmapause bulge associated with the flow stagnation point is sometimes located well into the post-dusk quadrant. The electric field models adopted by Knudsen [1974] and by Watkins [1978], on the other hand, were characterized by flow stagnation points located near the dusk meridian. Sojka et al. [1979] have examined the effect on high-latitude plasma convection of displacing the geomagnetic and geographic poles. They find that in the geographic inertial frame the main region of very low speed plasma flow is not confined to the dusk region but moves from early afternoon to near midnight during the course of a day.

The purpose of this section is to examine convection in the trough region using mid-latitude plasma flow trajectories computed from our time-dependent substorm simulation. As shown in the previous sections our computed electric field results are in good agreement with available measurements of average substorm-associated electric fields except in a restricted local time region near noon.

Figure 10 illustrates the instantaneous ionospheric electric

equipotential patterns computed for two times during the event we have simulated. The spacing between adjacent contours is 6 kV, and the contours are shown in a fixed, non-rotating coordinate system. Figure 10a (0900 UT) gives the ionospheric electric equipotential pattern at the end of the pre-growth phase quiet period, while Figure 10b (1050 UT) gives the equipotential pattern at substorm maximum. Since the direction of $\underline{E} \times \underline{B}/B^2$ plasma drift is perpendicular to $\underline{E}$, the equipotentials shown in Figure 10 also represent instantaneous drift paths for cold ionospheric plasma.

The curve labelled "saddle point contour" separates the region dominated by the corotation electric field from the higher latitude region where the magnetospheric convection electric field dominates. If the electric field pattern were steady for several days this curve would also correspond to the ionospheric projection of the plasmapause [Nishida, 1966]. Equatorward of this boundary, plasma flux tubes drift eastward on closed drift paths around the earth, while poleward of the boundary flux tubes participate in antisunward drift across the polar cap and sunward return flow at lower latitudes in the evening and morning auroral zones. Equipotential contours are not shown in the polar cap region of Figure 10 because this region is outside of the area we model. (See Paper 1).

In the pre-substorm case shown in Figure 10a, a flow stagnation point (equipotential saddle point) is found near 1500 LT. In the vicinity of this point the electric field is small and plasma drifts only slowly. By 1050 UT (Figure 10b) the stagnation point is located well into the nighttime sector near midnight. Following the arguments presented by Spiro et al. [1978], the trough would be expected to form by plasma decay

during the long time required for plasma flux tubes in the vicinity of the saddle point contour to drift eastward in approaching the nighttime stagnation point. The depleted flux tubes subsequently reverse their flow direction and begin to drift westward in agreement with Atmosphere Explorer-C ion drift velocity measurements made in the trough region [Spiro et al., 1978].

However, it must be remembered that Figure 10 gives only a "snapshot" of the instantaneous ionospheric drift pattern. As a result of the time dependent nature of substorm electric fields one cannot follow a given equipotential in Figure 10 to determine from where a given plasma flux tube has come or to where it will drift. In order to answer such questions it is necessary to consider the time dependent nature of the electric field.

Figure 11 shows computed $\underline{E} \times \underline{B}/B^2$ drift trajectories for plasma flux tubes that are located along the 1830 local time meridian at 1300 UT. Since our detailed substorm simulation only covers the four hour period from 0900 to 1300 UT, we have assumed that the pre-substorm (i.e., before 0900 UT) electric field pattern was time stationary and identical to the 0900 UT pattern. It should be emphasized that the flow trajectories shown in this figure do not correspond to instantaneous electric equipotentials at 1300 UT or at any other time. Instead, the trajectories shown in Figure 11 were computed by integrating the $\underline{E} \times \underline{B}/B^2$ drift velocities of individual plasma flux tubes back in time from 1300 UT. The interval between dots along a given trajectory corresponds to the passage of 1/2 hour.

Three classes of trajectories are apparent in Figure 11. The first

group of trajectories (A and B in Figure 11) approach the 1830 LT meridian by nearly corotating eastward from earlier local times. Thus, plasma flux tubes moving along these trajectories drift eastward approximately 1/2 hour of local time in the 1/2 hour interval between dots.

The second set of drift trajectories (C, D, and E) represent plasma flux tubes that have drifted eastward past the dusk meridian at lower latitudes before reversing their flow from eastward to westward in the post-dusk sector. Spiro et al. [1978] have concluded that plasma recombination along flow trajectories of this type is responsible for the low plasma concentrations found in the mid-latitude trough. We let τ represent the time available for plasma recombination to occur in the absence of solar photoionization for plasma flux tubes located along the 1830 LT meridian at 1300 UT. For the lower latitude plasma flux tubes shown in Figure 11 (trajectories A and B), $\tau \sim .5$ hour. For the second class of trajectories (C, D, and E) τ ranges from ~ 1 hour for trajectory C to ~ 6 hours for trajectory E. Thus the plasma concentrations within these flux tubes have had longer to decay than in the corotating flux tubes found further equatorward.

The third class of drift trajectories shown in Figure 11 (F, G, and H) are followed by plasma flux tubes that arrive at the 1830 LT meridian by convecting antisunward across the polar cap and then westward through the nighttime auroral zone. Since the polar cap is outside of the region we model, the paths of these flux tubes are shown only after they leave the polar cap on the nightside of the earth. The large distances between dots indicate that plasma flux tubes drift rapidly to the west along

these trajectories. Plasma concentrations within this region would be expected to be enhanced as the result of energetic particle precipitation in the auroral zone.

The plasma flow trajectories shown in Figure 11 are in substantial agreement with the plasma flow pattern deduced from Atmosphere Explorer data by Spiro et al. [1978]. In order to assess the ionospheric effects of a substorm followed by a long recovery or of a series of repeated substorms and recoveries it is necessary to extend our present calculation to cover longer time periods. Presumably, as the mid-latitude electric field relaxes during substorm recovery, depleted plasma flux tubes drifting westward along trajectories C, D, and E might again become dominated by the corotation electric field and begin to drift back to the east. Thus, during periods of intermittent substorms and recoveries the trough would extend throughout the entire nighttime sector.

V. CONCLUSION

In this paper we have used some of the results of the quantitative substorm simulation presented in Papers 1 and 2 to investigate theoretically the penetration of substorm-associated electric fields into the plasmasphere and mid-latitude ionosphere. In agreement with recent whistler results presented by Park [1978] and Carpenter et al. [1979] we find that during substorms the evening local time sector is characterized by eastward electric field components (outward plasma drift), while the early morning sector is characterized by westward electric field

components (inward plasma drift). The largest discrepancies between our results and the whistler data occur near the noon meridian where our numerical procedure suffers from known inadequacies (see Paper 1). In addition, Carpenter et al., [1979] have pointed out that the substorm $\underline{E}$ pattern near noon resembles the quiet day pattern and might originate in a dynamo process. Such processes are presently not included in our model.

Our results offer reasonable agreement with east-west plasma drifts measured at St. Santin during magnetically disturbed periods [Blanc, 1978]; there are unresolved discrepancies, however, between the north-south drift component as measured at St. Santin and the north-south drift inferred from our electric field pattern.

The penetration of substorm electric fields into the plasmasphere can have dramatic effects on the temporal evolution of the plasmapause boundary. By assuming an initial location of the plasmapause and then integrating the $\underline{E} \times \underline{B}/B^2$ drift of plasma flux tubes from that boundary we conclude that long narrow filamentary tails can be drawn out from the dusk plasmasphere within the four hour substorm period that we model.

From investigation of the time-dependent flow of plasma in the mid-latitude ionosphere we conclude that some mid-latitude plasma flux tubes that drift eastward past the dusk terminator reverse their motion between dusk and midnight and begin to drift back to the west again toward the terminator. Spiro et al. [1978] have suggested that such flow trajectories are responsible for the formation of the mid-latitude ionization trough. The results presented in this paper indicate that such a plasma flow geometry could be due to substorm-associated changes in the global electric field pattern.

ACKNOWLEDGEMENTS

We would like to acknowledge enlightening dicussions with C. G. Park and F. Rich. In addition, we are grateful to D. L. Carpenter for helpful comments on an earlier draft of this work.

This work has been supported in part by the Atmospheric Sciences Section of the National Science Foundation under Grant ATM74-21185, by the U.S. Air Force Geophysics Laboratory under contract F19628-77-C-0005 and by the National Aeronautics and Space Administration under grant NGR-44-006-137.

REFERENCES

Banks, P. M., R. W. Schunk, and W. J. Raitt, NO^+ and O^+ in the high latitude F-region, Geophys. Res. Lett., 1, 239, 1974.

Binsack, J. H., Plasmapause observations with the M.I.T. experiment on IMP 2, J. Geophys. Res., 72, 5231, 1967.

Blanc, M., Midlatitude convection electric fields and their relation to ring current development, Geophys. Res. Lett., 5, 203, 1978.

Blanc, M., P. Amayenc, P. Bauer, and C. Taieb, Electric field induced drifts from the French incoherent scatter facility, J. Geophys. Res., 82, 87, 1977.

Block, L. P., On the distribution of electric fields in the magnetosphere, J. Geophys. Res., 71, 855, 1966.

Carpenter, D. L., Whistler evidence of a knee in the magnetospheric ionization density profile, J. Geophys. Res., 68, 1675, 1963.

Carpenter, D. L., Whistler studies of the plasmapause in the magnetosphere, 1, Temporal variations in the position of the knee and some evidence on plasma motions near the knee, J. Geophys. Res., 71, 693, 1966.

Carpenter, D. L., Relations between the dawn minimum in the equatorial radius of the plasmapause and Dst, Kp, and local K at Byrd Station, J. Geophys. Res., 72, 2969, 1967.

Carpenter, D. L., Whistler evidence of the dynamic behavior of the duskside bulge in the plasmasphere, J. Geophys. Res., 75, 3837, 1970.

Carpenter, D. L., and C. G. Park, On what ionospheric workers should know about the plasmapause-plasmasphere, Rev. Geophys. Space Phys., 11, 133, 1973.

Carpenter, D. L., and N. T. Seely, Cross-L plasma drifts in the outer plasmasphere: Quiet time patterns and some substorm effects, J. Geophys. Res., 81, 2728, 1976.

Carpenter, D. L., K. Stone, J. C. Siren, and T. L. Crystal, Magnetospheric electric fields deduced from drifting whistler paths, J. Geophys. Res., 77, 2819, 1972.

Carpenter, D. L., C. G. Park, and T. R. Miller, A model of substorm electric fields in the plasmasphere based on whistler data, J. Geophys. Res., 84, 6559, 1979.

Chappell, C. R., K. K. Harris, and G. W. Sharp, A study of the influence of magnetic activity on the location of the plasmapause as measured by Ogo 5, J. Geophys. Res., 75, 50, 1970.

Chappell, C. R., Recent satellite measurements of the morphology and dynamics of the plasmasphere, Rev. Geophys. Space Phys., 10, 951, 1972.

Chappell, C. R., Detached plasma regions in the magnetosphere, J. Geophys. Res., 79, 1861, 1974.

Chen, A. J., and R. A. Wolf, Effects on the plasmasphere of a time-varying convection electric field, Planet. Space Sci., 20, 483, 1972.

Chen, A. J., and J. M. Grebowsky, Plasma tail interpretations of pronounced detached plasma regions measured by Ogo 5, J. Geophys. Res., 79, 3851, 1974.

Chen, A. J., J. M. Grebowsky, and H. A. Taylor, Jr., Dyanmics of mid-latitude light ion trough and plasma tails, J. Geophys. Res., 80, 968, 1975.

Evans, J. V., Measurements of horizontal drifts in the E and F region at Millstone Hill, J. Geophys. Res., 77, 2341, 1972.

Evans, J. V., A review of F region dynamics, Rev. Geophys. Space Phys., 13, 887, 1975.

Fejer, B. G., C. A. Gonzales, D. T. Farley, M. C. Kelley and R. F. Woodman, Equatorial electric fields during magnetically disturbed conditions, 1, The effect of the interplanetary magnetic field, J. Geophys. Res., 84, 5797, 1979.

Gonzales, C. A., M. C. Kelley, B. G. Fejer, J. F. Vickrey and R. F. Woodman, Equatorial electric fields during magnetically disturbed conditions, 2, Implications of simultaneous auroral and equatorial measurements, J. Geophys. Res., 84, 5803, 1979.

Grebowsky, J. M., Model study of plasmapause motion, J. Geophys. Res., 75, 4329, 1970.

Grebowsky, J. M., Time-dependent plasmapause motion, J. Geophys. Res., 76, 6193, 1971.

Grebowsky, J. M., Y. K. Tulunay, and A. J. Chen, Temporal variations in the dawn and dusk midlatitude trough and plasmapause positions, Planet. Space Sci., 22, 1089, 1974.

Grebowsky, J. M., J. H. Hoffman, and N. C. Maynard, Ionospheric and magnetospheric 'plasmapauses', Planet. Space Sci., 26, 651, 1978.

Gringauz, K. I., The structure of the ionized gas envelope of earth from direct measurements in the U.S.S.R. of local charged particle concentrations, Planet. Space Sci., 11, 281, 1963.

Harel, M., and R. A. Wolf, Convection, in Physics of Solar-Planetary Environments, Vol. II, ed. by D. J. Williams, American Geophysical Union, Washington, D. C., p. 617, 1976.

Harel, M., R. A. Wolf, P. H. Reiff, R. W. Spiro, W. J. Burke, F. J. Rich, and M. Smiddy, Quantitative simulation of a magnetospheric substorm, 1., Model logic and overview, J. Geophys. Res., this issue.

Harel, M., R. A. Wolf, R. W. Spiro, P. H. Reiff, C.-K. Chen, W. J. Burke, F. J. Rich, and M. Smiddy, Quantitative simulation of a magnetospheric substorm, 2., Comparison with observations, J. Geophys. Res., this issue.

Jaggi, R. K., and R. A. Wolf, Self-consistent calculation of the motion of a sheet of ions in the magnetosphere, J. Geophys. Res., 78, 2852, 1973.

Karlson, E. T., Streaming of a plasma through a magnetic dipole field, Phys. Fluids, 6, 708, 1963.

Karlson, E. T., Plasma flow in the magnetosphere, 1, A 2-dimensional model of stationary flow, Cosmic Electrodyn., 1, 474, 1971.

Kelley, M. C., B. G. Fejer, and C. A. Gonzales, An explanation for anomalous equatorial ionospheric electric fields associated with a northward turning of the interplanetary magnetic field, Geophys. Res. Letter, 6, 301, 1979.

Kivelson, M. G., Magnetospheric electric fields and their variation with geomagnetic activity, Rev. Geophys. Space Phys., 14, 189, 1976.

Knudsen, W. C., Magnetospheric convection and the high-latitude F ionosphere, J. Geophys. Res., 79, 1046, 1974.

Lemaire, J., The mechanisms of formation of the plasmapause, Ann. Geophys. 31, 175, 1975.

Mozer, F. S., Electric fields and plasma convection in the plasmasphere, Rev. Geophys. Space Phys., 11, 755, 1973.

Muldrew, D. B., F-layer ionization troughs deduced from Alouette data, J. Geophys. Res., 70, 2635, 1965.

Nishida, A., Formation of the plasmapause or magnetospheric plasma knee by the combined action of magnetospheric convection and plasma escape from the tail, J. Geophys. Res., 71, 5667, 1966.

Park, C. G., Whistler observations of the interchange of ionization between the ionosphere and the protonosphere, J. Geophys. Res., 75, 4249, 1970.

Park, C. G., Westward electric fields as the cause of nighttime enhancements in electron concentrations in midlatitude F region, J. Geophys. Res., 76, 4560, 1971.

Park, C. G., Whistler observations of substorm electric fields in the nightside plasmasphere, J. Geophys. Res., 83, 5773, 1978.

Park, C. G., and C.-I. Meng, Vertical motions of the midlatitude F layer during magnetospheric substorms, J. Geophys. Res., 76, 8326, 1971.

Park, C. G., and C.-I. Meng, Distortions of the nightside ionosphere during magnetospheric substorms, J. Geophys. Res., 78, 3828, 1973.

Schunk, R. W., W. J. Raitt, and P. M. Banks, Effect of electric fields on the daytime high latitude E and F regions, J. Geophys. Res., 80, 3121, 1975.

Schunk, R. W., P. M. Banks, and W. J. Raitt, Effects of electric fields and other processes upon the nighttime high-latitude F layer, J. Geophys. Res., 81, 3271, 1976.

Sharp, G. W., Mid-latitude trough in the night ionosphere, J. Geophys. Res., 71, 1345, 1966.

Sojka, J. J., W. J. Raitt, and R. W. Schunk, Effect of displaced geomagnetic and geographic poles on high-latitude plasma convection and ionospheric depletions, J. Geophys. Res., 84, 5943, 1979.

Spiro, R. W., A study of plasma flow in the mid-latitude ionization trough, Ph.D. thesis, University of Texas at Dallas, 1978.

Spiro, R. W., R. A. Heelis, and W. B. Hanson, Ion convection and the formation of the mid-latitude F-region ionization trough, J. Geophys. Res., 83, 4255, 1978.

Swift, D. W., Possible mechanisms for formation of the ring current belt, J. Geophys. Res., 76, 2276, 1971.

Taylor, H. A., H. C. Brinton, and C. R. Smith, Positive ion composition in the magnetoionosphere obtained from the Ogo-A satellite, J. Geophys. Res., 70, 5769, 1965.

Taylor, H. A., H. C. Brinton, D. L. Carpenter, F. M. Bonner, and R. L. Heyborne, Ion depletion in the high latitude exosphere: simultaneous OGO-2 observations of the light ion trough and the VLF cut-off, J. Geophys. Res., 74, 3517, 1969.

Taylor, H. A., The light-ion trough, Planet. Space Sci., 20, 1593, 1972.

Testud, J., P. Amayenc, and M. Blanc, Middle and low latitude effects of auroral disturbances from incoherent-scatter, J. Atmos. Terr. Phys., 37, 989, 1975.

Titheridge, J. E., Plasmapause effects in the top side ionosphere, J. Geophys. Res., 81, 3227, 1976.

Vasyliunas, V. M., Mathematical models of magnetospheric convection and its coupling to the ionosphere, in Particles and Fields in the Magnetosphere, ed. by B. M. McCormac, p. 60, D. Reidel, Dordrecht. Netherlands, 1970.

Vasyliunas, V. M., The interrelationship of magnetospheric processes, in Earth's Magnetospheric Processes, ed. by B. M. McCormac, p. 29, D. Reidel, Dordrecht, Netherlands, 1972.

Watkins, B. J., A numerical computer investigation of the polar F-region ionosphere, Planet. Space Sci., 26, 559, 1978.

Wolf, R. A., Effects of ionospheric conductivity on convective flow of plasma in the magnetosphere, J. Geophys. Res., 75, 4677, 1970.

FIGURE CAPTIONS

Figure 1 Computed eastward electric field at $4R_E$ in magnetospheric equatorial plane as function of local time. The eastward field components at the end of the pre-substorm quiet period (0900 UT), just before substorm onset (1000-εUT) and just after onset (1000+εUT) are shown in a), while the components at substorm maximum (1050 UT), at the time of maximum measured cross-polar-cap potential drop (1150 UT), and at a time during the recovery phase of the modeled event (1300 UT) are shown in b). Eastward $\underline{E}$ corresponds to outward $\underline{E} \times \underline{B}/B^2$ drift in the equatorial plane, and westward $\underline{E}$ corresponds to inward drift.

Figure 2 Same as Figure 1 except that the computed radial electric field components are shown in a reference frame that corotates with the earth. Radially outward $\underline{E}$ corresponds to westward $\underline{E} \times \underline{B}/B^2$ drift, while inward-directed equatorial $\underline{E}$ corresponds to eastward drift.

Figure 3 Computed eastward electric field components in the ionosphere at 1050 UT for 60°, 50°, 40°, and 30 latitude. Eastward $\underline{E}$ corresponds to regions of poleward $\underline{E} \times \underline{B}/B^2$ drift, while westward $\underline{E}$ corresponds to equatorward drift.

Figure 4 Same as Figure 3 except the computed equatorward electric field components are shown in a reference frame that corotates with the earth.

Figure 5 Electric equipotential pattern in equatorial plane of magnetosphere at 1050 UT. The view is looking down on the equatorial plane with the sun to the left and dusk at the bottom. Adjacent equipotentials differ by 6 kV. The abrupt ionosphere conductivity changes at dawn and dusk are responsible for the larger duskside potential drop vis a vis the dawnside and lead to the characteristic field pattern illustrated in Figures 1-4.

Figure 6 Comparison of average eastward E component near 4 R_E as determined by the cross-L motion of whistler ducts during disturbed periods [Carpenter et al., 1979] and the average of our computed substorm-associated eastward E component at $4R_E$.

Figure 7 Comparison of average poleward ionospheric E component scaled from St. Santin radar data presented by Blanc [1978] and the average of our computed substorm-associated poleward E component at 50° in the ionosphere.

Figure 8 Temporal evolution of the plasmapause from an assumed initial configuration derived from the last closed

equipotential at 0900 UT. The view is looking down on the magnetospheric equatorial plane with the sun to the left and dusk at the bottom. The time development of the plasmapause is computed by following the $\underline{E} \times \underline{B}/B^2$ drift motion of plasma flux tubes from the initial boundary. Within one hour of substorm onset the initial afternoon plasmapause bluge drifts out to the dayside magnetopause and a secondary plasma tail begins to form near dusk.

Figure 9 Same as Figure 8 except the initial plasmapause is assumed to map to a circle at 55° latitude in the ionosphere. Note that although a post-dusk bulge is apparent in the location of the boundary by 1100 UT a well-defined plasmatail does not form near dusk for this case.

Figure 10 Computed electric equipotential contours in the equatorial plane of the magnetosphere at a) the end of the pre-substorm quiet period and b) the time of substorm maximum. The contours are shown in a fixed, non-rotating reference frame with adjacent contours separated by 6 kV. The curve labelled "saddle point contour" separates the region dominated by the corotation electric field from the higher latitude region where the magnetospheric convection electric field dominates.

Figure 11 Computed drift trajectories of plasma flux tubes located along the 1830 LT meridian at 1300 UT. The interval between dots along a given trajectory corresponds to the passage of 1/2 hour.

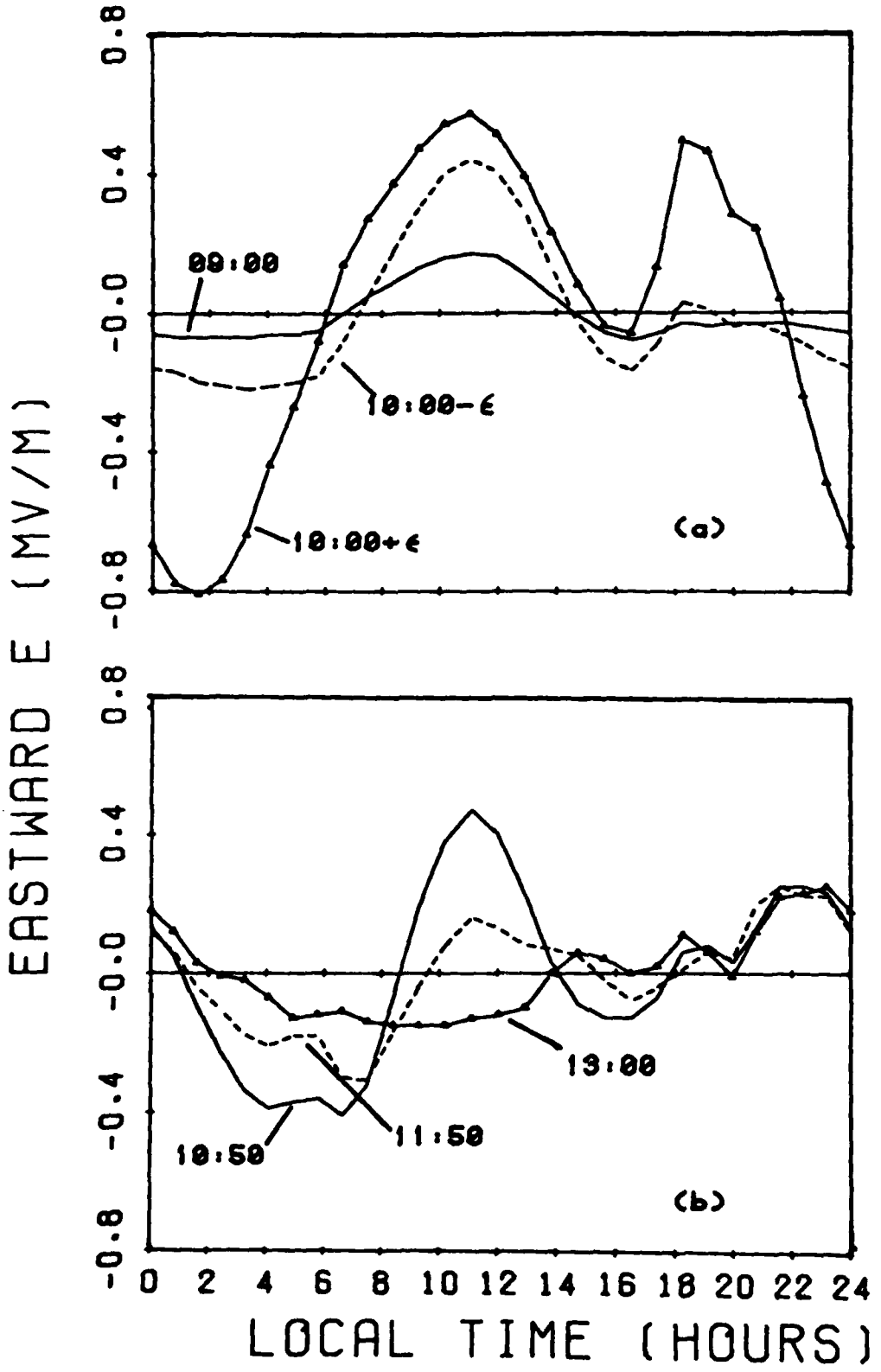
EASTWARD E (MV/M)
0.8
0.4
-0.0
-0.4
-0.8
00:00
10:00-ε
10:00+ε
(a)
13:00
11:50
10:50
(b)
0 2 4 6 8 10 12 14 16 18 20 22 24
LOCAL TIME (HOURS)

Figure 1

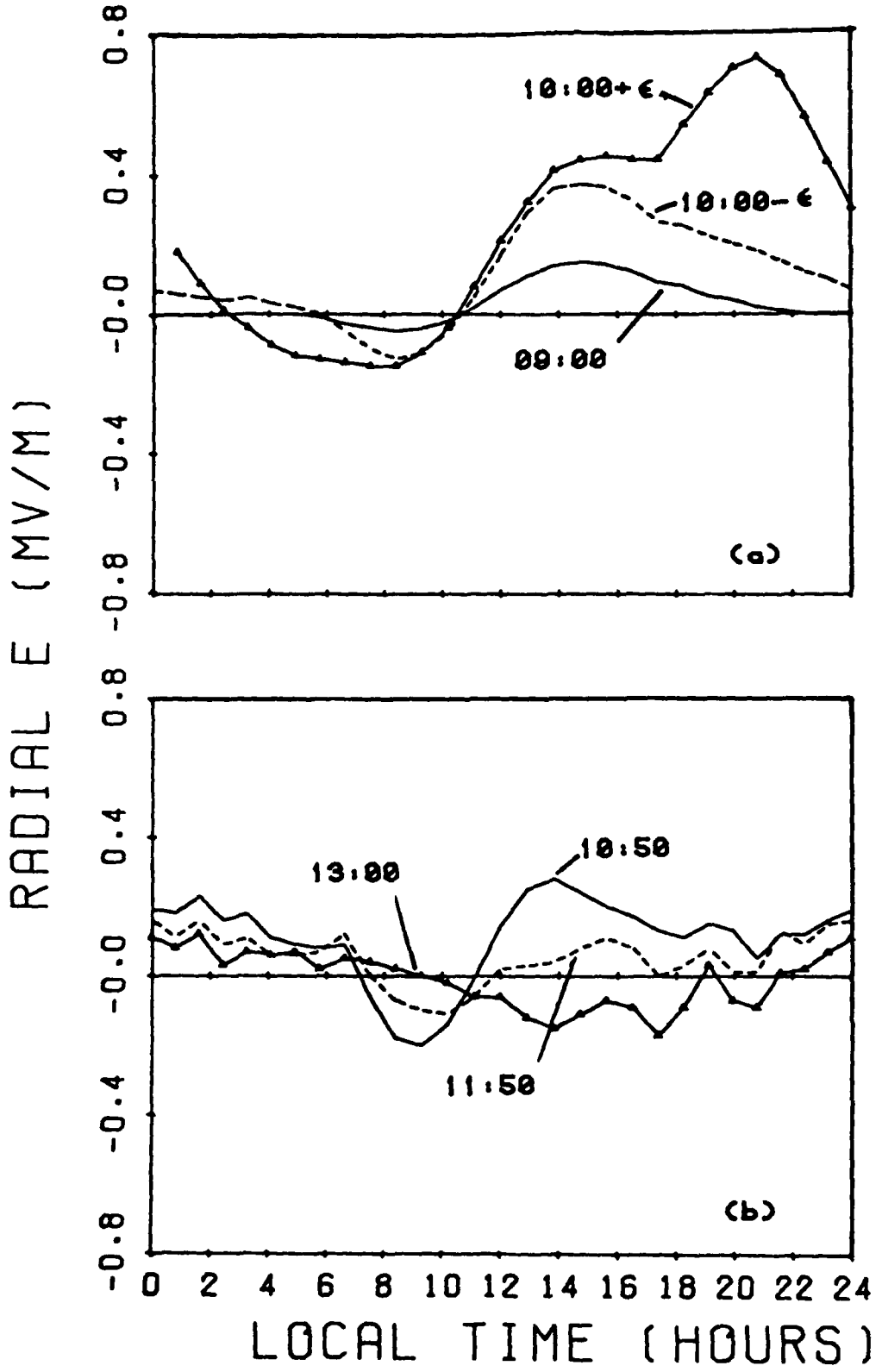
RADIAL E (MV/M)
0.8
0.4
-0.0
-0.4
-0.8
10:00+ϵ
10:00-ϵ
09:00
(a)
13:00
10:50
11:50
(b)
0 2 4 6 8 10 12 14 16 18 20 22 24
LOCAL TIME (HOURS)

Figure 2

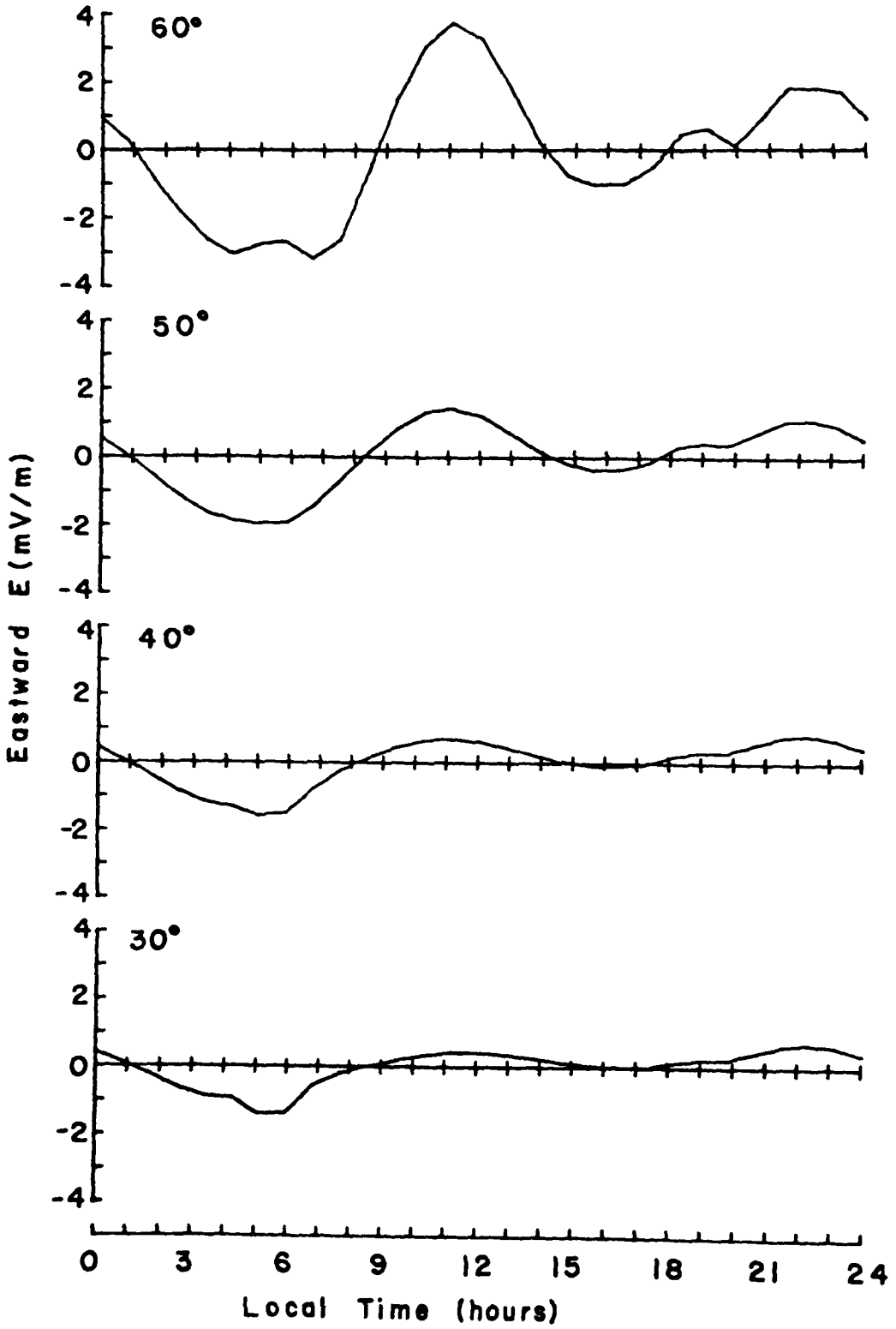
60°
50°
40°
30°
4
2
0
-2
-4
Eastward E (mV/m)
0
3
6
9
12
15
18
21
24
Local Time (hours)

Figure 3

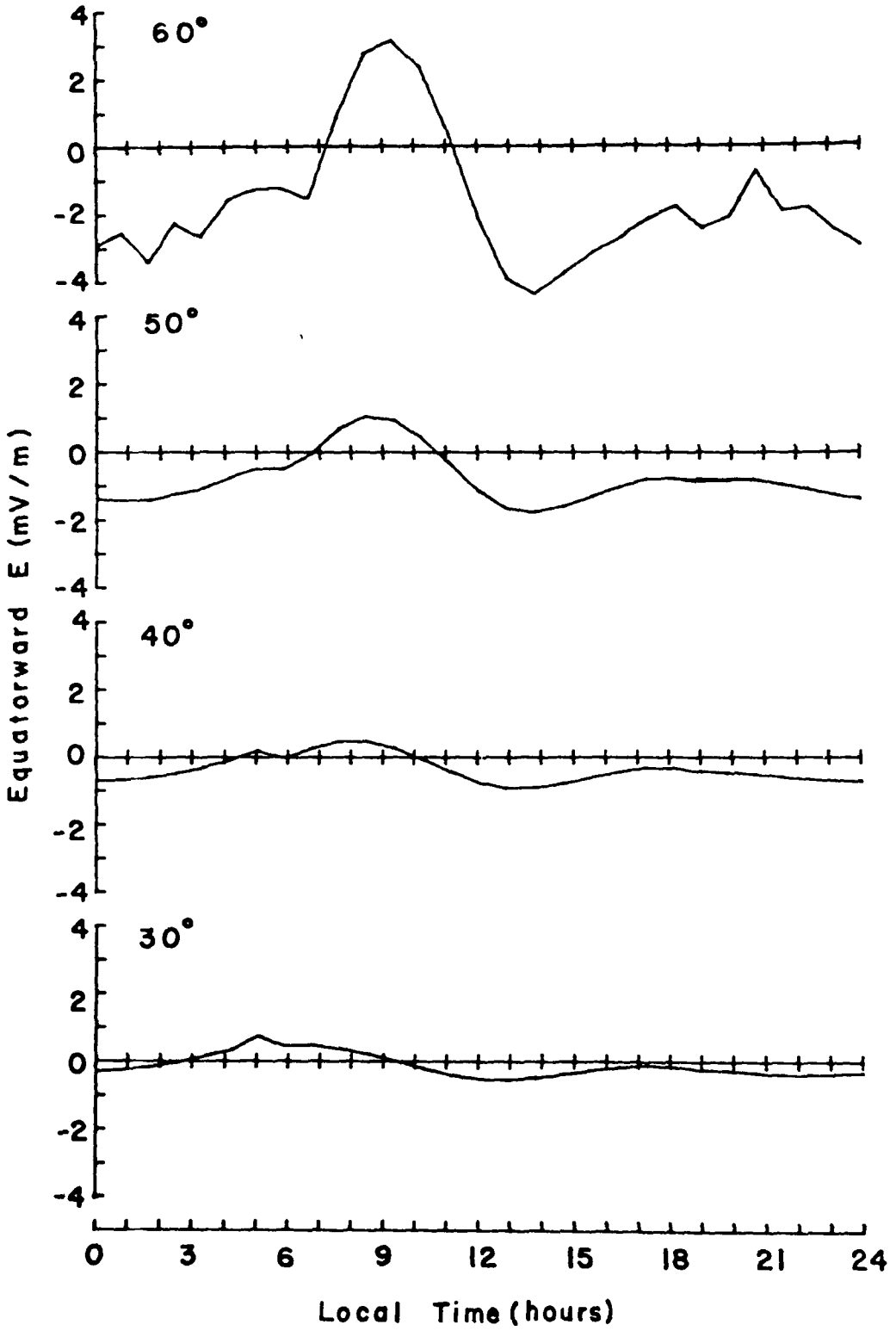
60°
50°
40°
30°
4
2
0
-2
-4
Equatorward E (mV/m)
0
3
6
9
12
15
18
21
24
Local Time (hours)

Figure 4

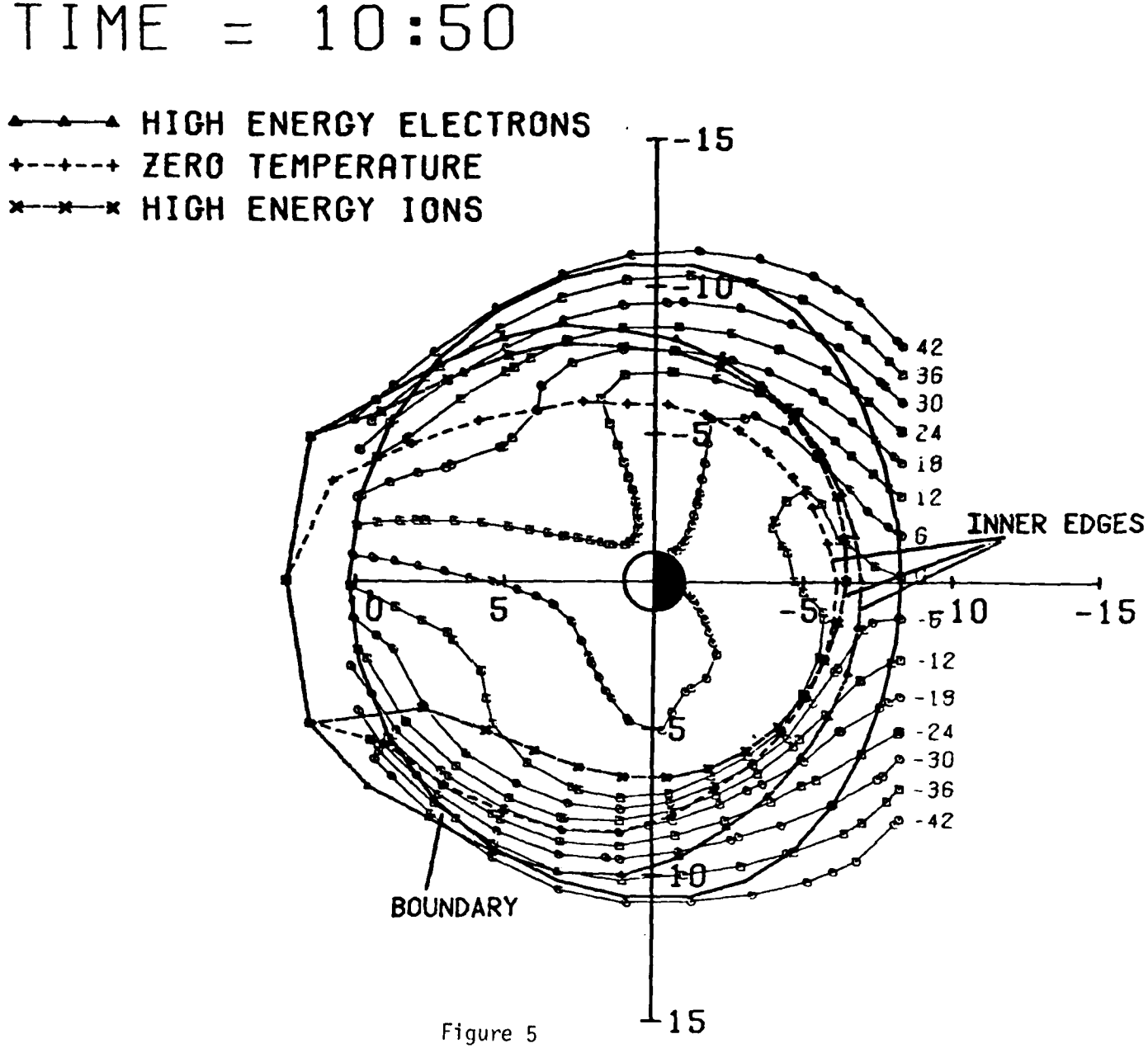
TIME = 10:50
HIGH ENERGY ELECTRONS
ZERO TEMPERATURE
HIGH ENERGY IONS
-15
-10
-5
5
10
15
0
5
-5
-10
42
36
30
24
18
12
6
-6
-12
-18
-24
-30
-36
-42
INNER EDGES
BOUNDARY

Figure 5

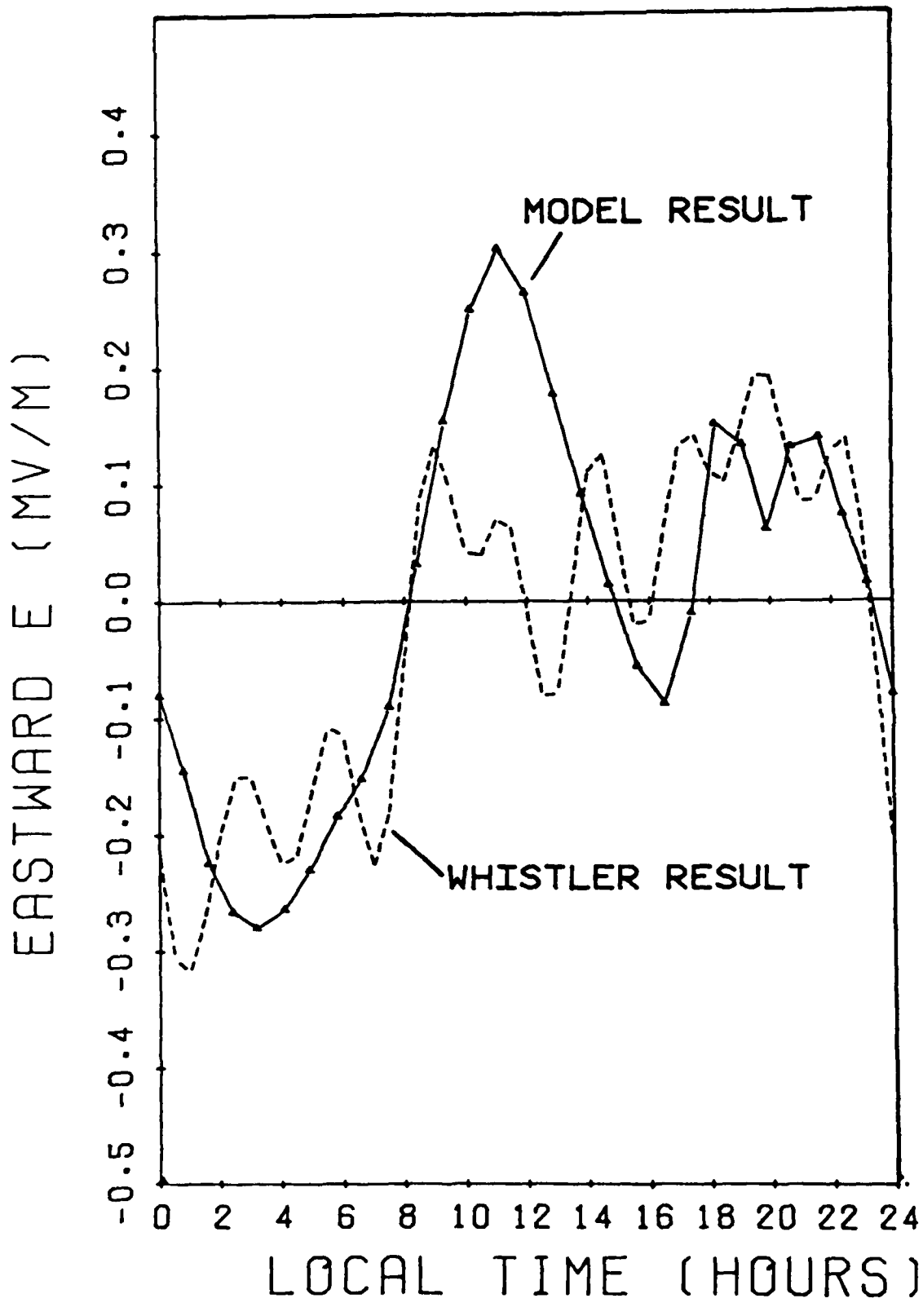
MODEL RESULT
WHISTLER RESULT
EASTWARD E (MV/M)
-0.5 -0.4 -0.3 -0.2 -0.1 0.0 0.1 0.2 0.3 0.4
0 2 4 6 8 10 12 14 16 18 20 22 24
LOCAL TIME (HOURS)

Figure 6

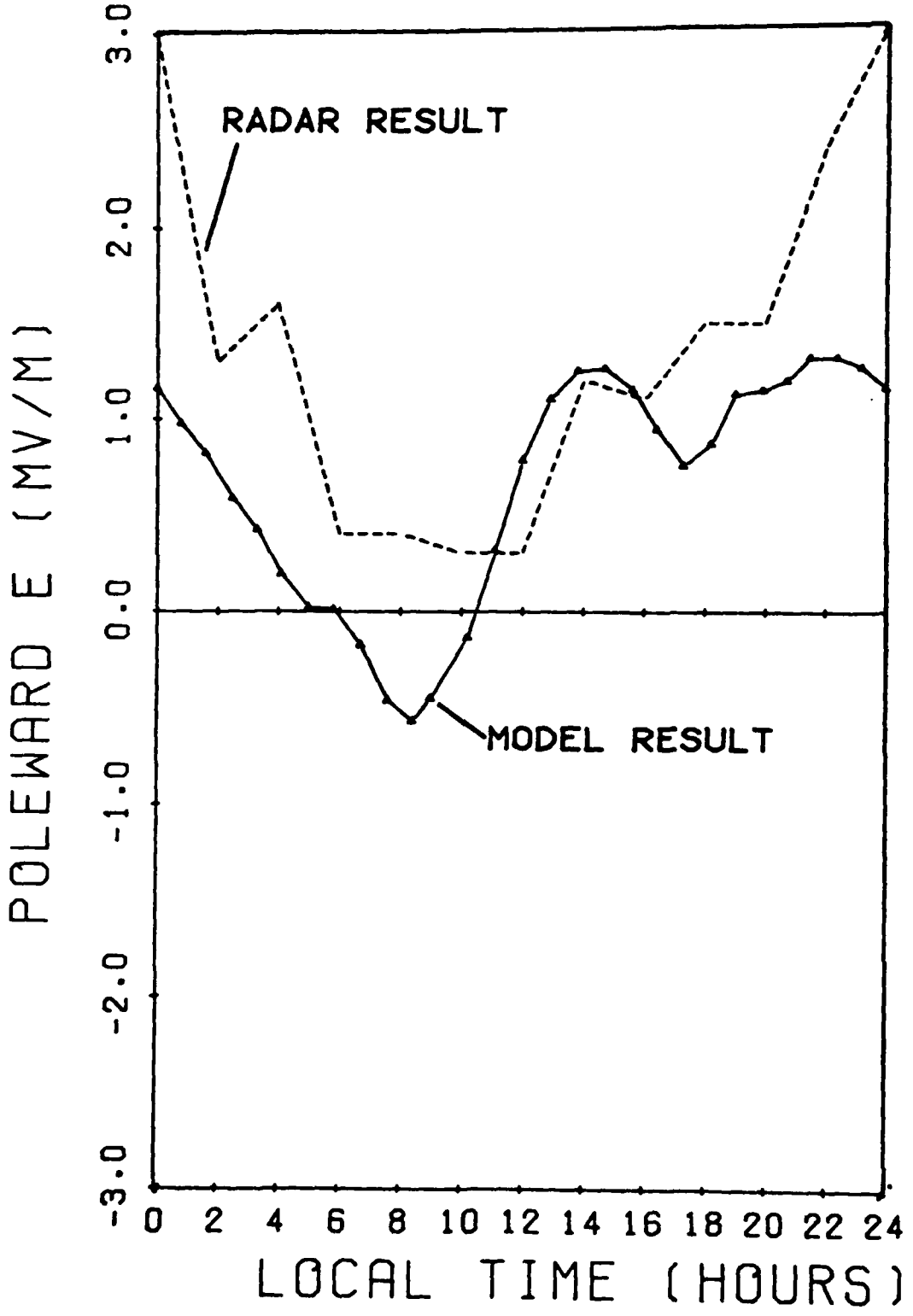
RADAR RESULT
MODEL RESULT
POLEWARD E (MV/M)
3.0
2.0
1.0
0.0
-1.0
-2.0
-3.0
0 2 4 6 8 10 12 14 16 18 20 22 24
LOCAL TIME (HOURS)

Figure 7

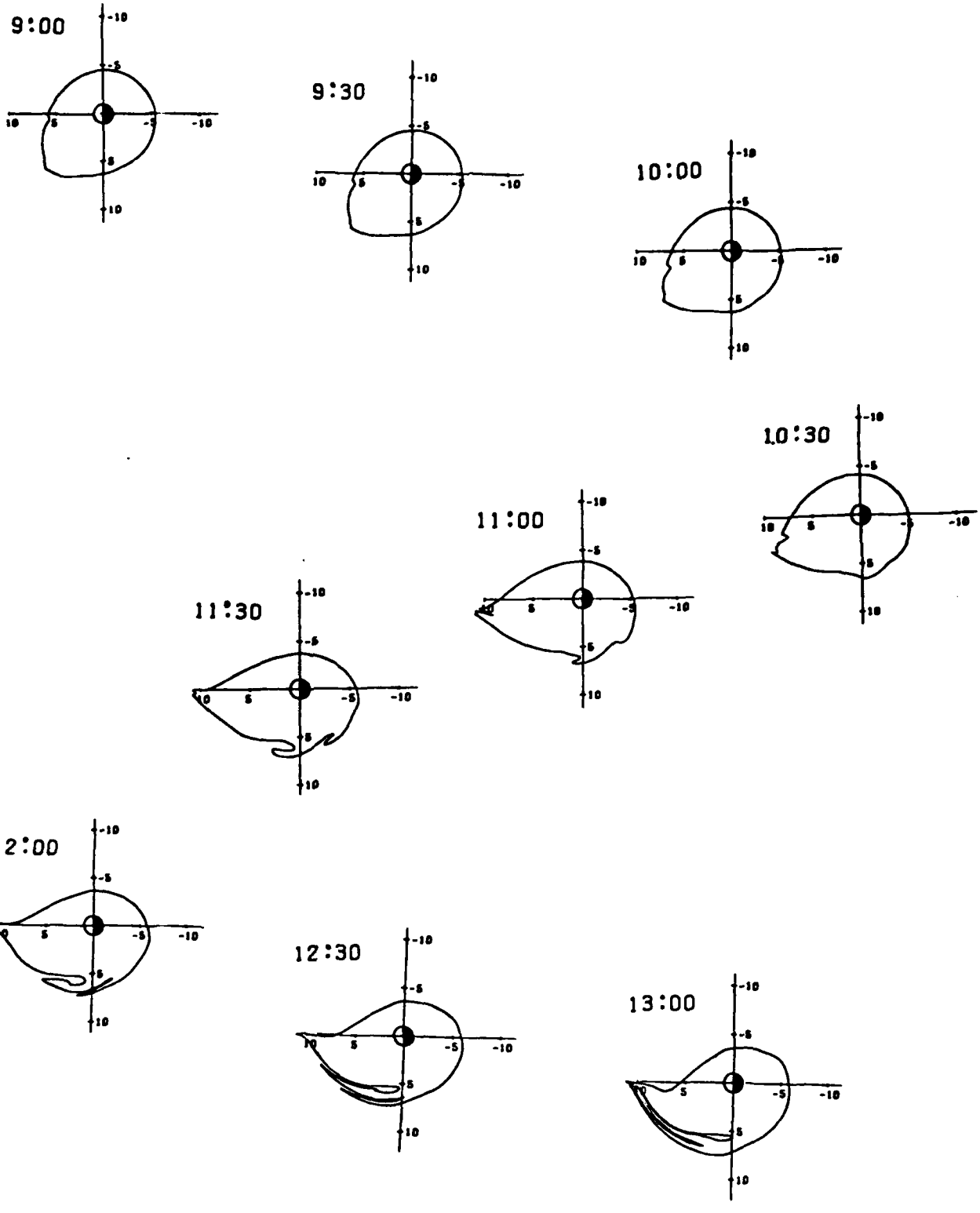

Figure 3

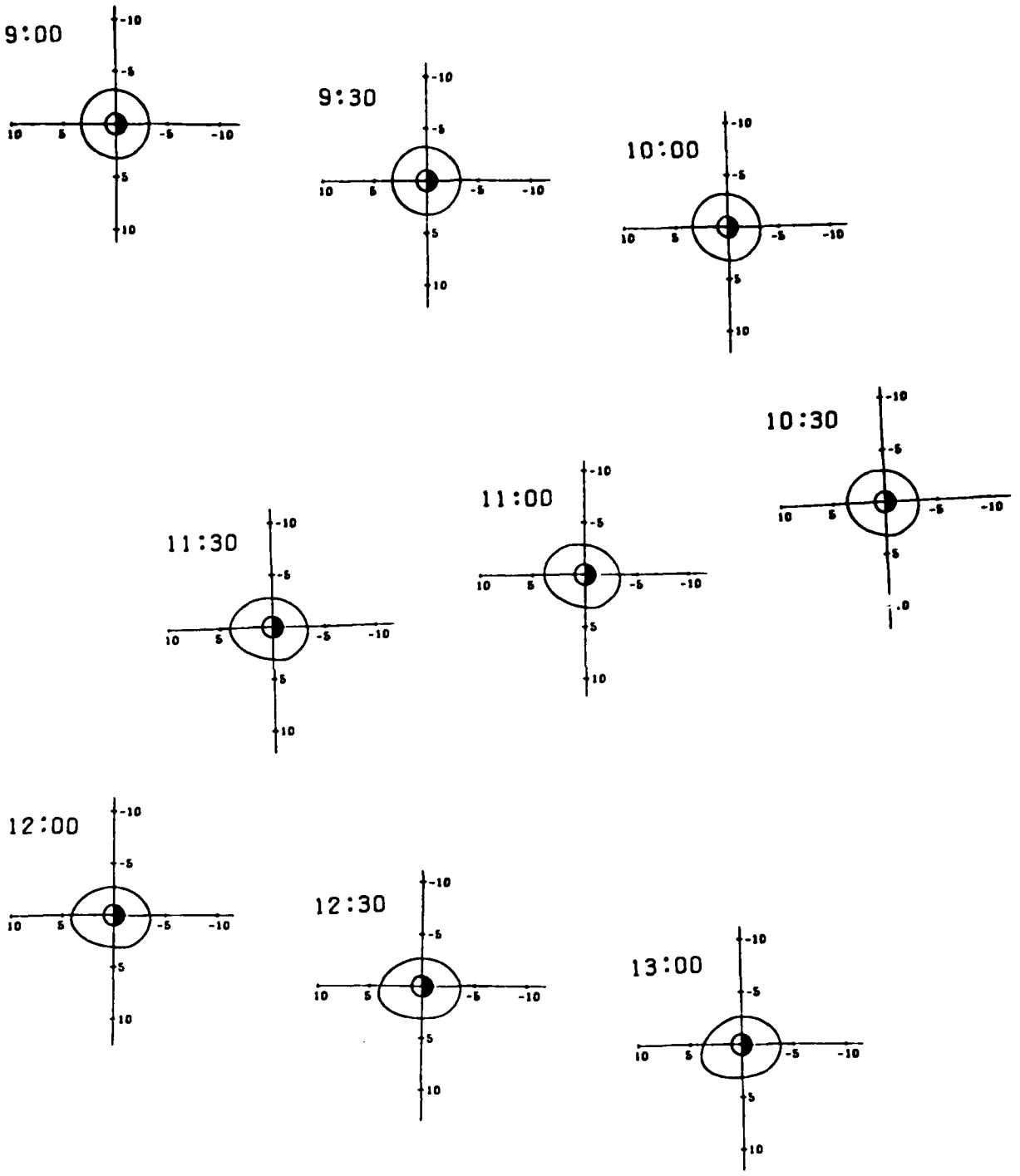

Figure 9

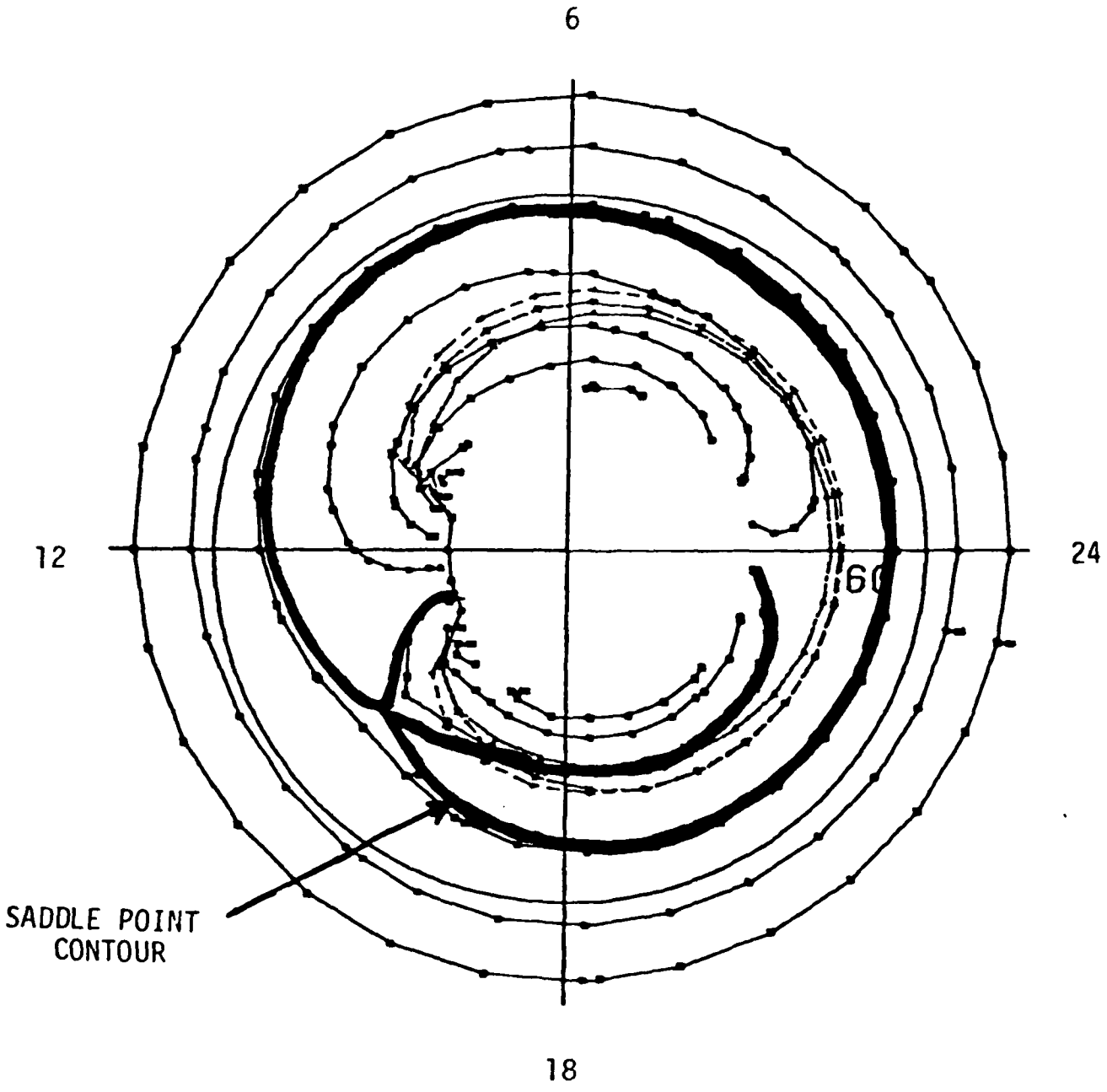

Figure 10a

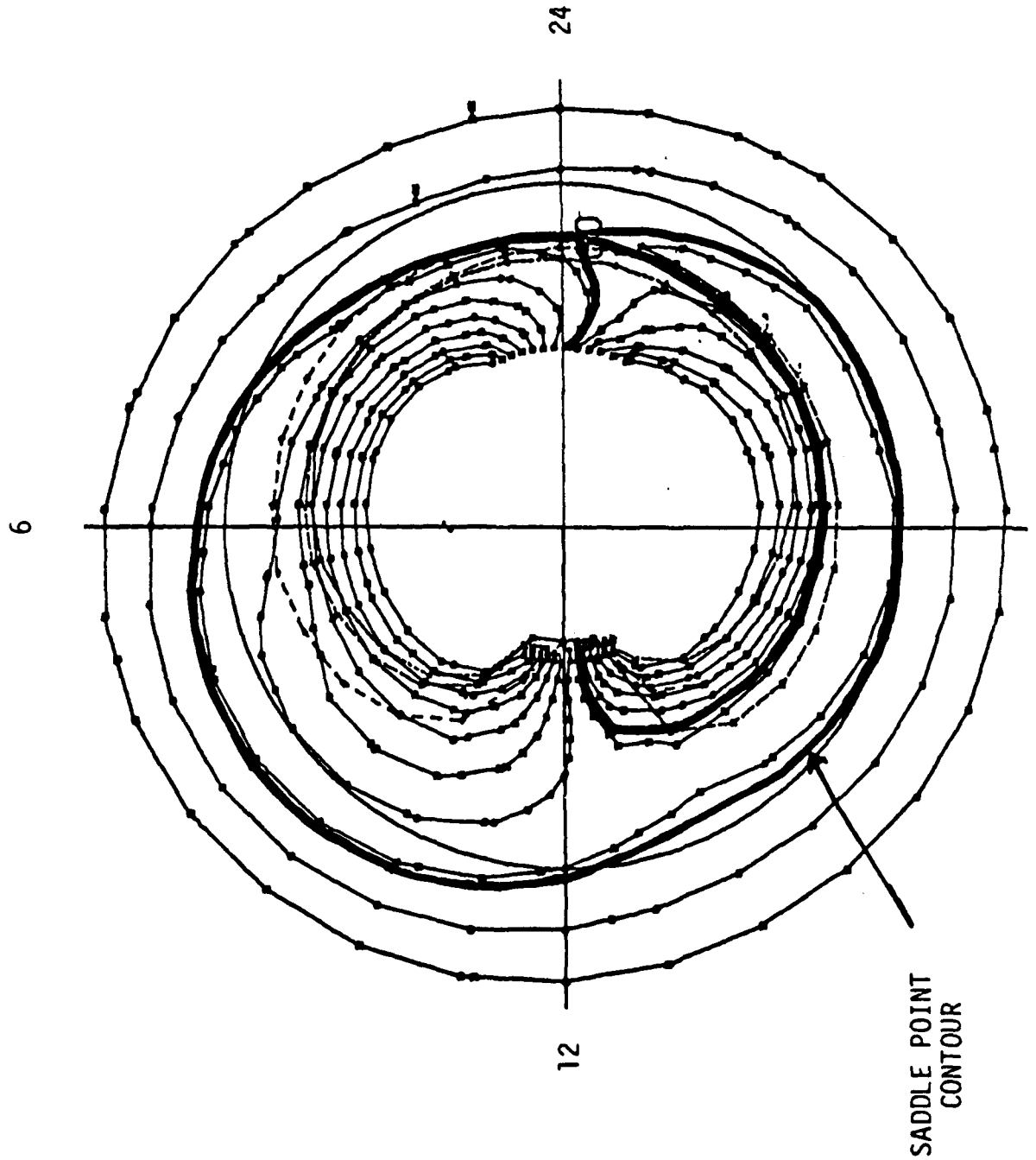

Figure 10b

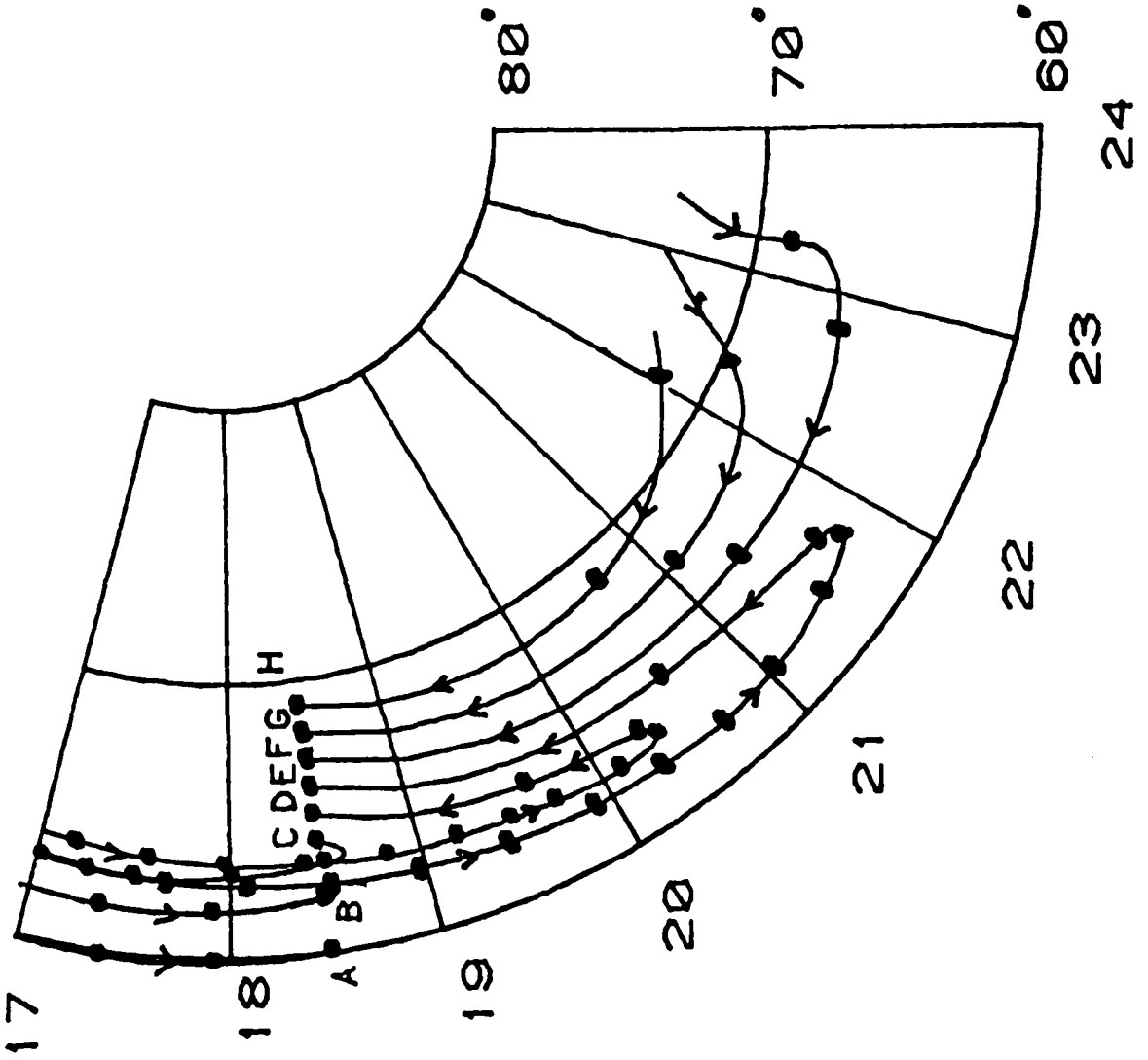

Figure 11